PAPER

Mapping graphene layer number at few-micron-scale spatial resolution over large areas using laser scanning

To cite this article: Amanda J Carr et al 2021 2D Mater. 8 025001

View the <u>article online</u> for updates and enhancements.

2D Materials



RECEIVED

17 September 2020

REVISED

9 November 2020

ACCEPTED FOR PUBLICATION 18 November 2020

PUBLISHED

17 December 2020

PAPER

Mapping graphene layer number at few-micron-scale spatial resolution over large areas using laser scanning

Amanda J Carr^{1,2}, Daniel DeGennaro³, Joseph Andrade⁴, Alexander Barrett⁵, Surita R Bhatia¹ and Matthew D Eisaman³

- ¹ Department of Chemistry, Stony Brook University, Stony Brook, NY, United States of America
- Current address: Chemical Sciences and Engineering Division, Argonne National Laboratory, IL
- Department of Electrical and Computer Engineering, Stony Brook University, Stony Brook, NY, United States of America
- Department of Physics, Stony Brook University, Stony Brook, NY, United States of America
- ⁵ Department of Applied Mathematics, Harvard, Cambridge, MA, United States of America

E-mail: matthew.eisaman@stonybrook.edu

Keywords: single layer graphene, multilayer graphene, visualization, optical transmission, graphene coverage Supplementary material for this article is available online

Abstract

In-line graphene characterization to determine quality, area coverage fraction, and layer number on transparent substrates is critical to large-scale commercial graphene production. Many applications, including biosensors and imbedded diagnostics, flexible electronics, and transparent electrodes, require uniform graphene transfer from its native chemical vapor deposition foil to transparent films. To enable high-volume production of these devices, graphene layer number, quality, and area coverage must be mapped at high spatial resolution to enable growth and transfer process optimization. To this end, we present a spatially resolved optical transmission technique combined with statistical analysis of the measurements to determine graphene layer number on different transparent substrates, including polymer films and glass. This method can be automated and does not require user-inputted threshold values. Our method can effectively map >1 cm² areas at 10 micron resolution and is not limited by type of substrate or thickness assuming the substrate is transparent. We corroborate these experimental results with simulated data and present guidelines to reasonably assess graphene quality, layer number, and feature size as functions of the experimental parameters.

1. Introduction

The realization of commercial graphene products, including biointerfaces [1–3], flexible electronics [4–6], and transparent electrodes [4, 7, 8], requires large-scale characterization of graphene across the target substrate area to assess graphene quality and coverage. Currently, roll-to-roll chemical vapor deposition (CVD) of graphene onto metal foil, followed by graphene transfer to the ultimate target substrate is the most promising route to commercial graphene device production [9]. CVD is a tunable process that can produce the uniform, large-area graphene sheets needed for device fabrication [10]. Maximizing the fidelity of transfer to the target substrate and minimizing damage during the transfer process are critical to scaling this technology up to

large areas and commercial volumes [11]. Useful efforts have made graphene detection on these native metal foils possible via thermal annealing [12] and plasma etching [13]. Additionally, post-transfer spatial mapping of layer number can provide information on the spatial homogeneity of layer number during the growth process. Recent research advances have significantly reduced contamination during transfer [14, 15] and have introduced metal foil recyclability [16, 17]. Because the electronic and mechanical properties of graphene depend highly on the number of layers present and the overall graphene quality [18-20], the final graphene/substrate stack must be thoroughly characterized to enable feedback and ultimate process optimization of the manufacturing and transfer parameters. To this end, we present a simple, non-destructive, spatially resolved optical method to characterize graphene layer number on transparent substrates. In this paper, we present results using a rastered laser but similar data and spatial information can be obtained in a single-shot measurement using a pixelated image sensor with a large area. This single-shot variation of our technique may be more conducive to integration as in-line quality control and feedback in a commercial manufacturing process.

The optical properties of graphene have been well established both experimentally and theoretically. Single layer graphene absorbs 2.3% of incident light across nearly all visible frequencies [21–24] and absorbance is governed by fine structure constant [25]. UV absorbance is considerably higher [26]. Visible absorbance follows layer number linearly for up to \sim 10 layers after which additional absorbance per layer tapers off [27]. Groups have proposed models to predict transmission based on layer number [28], substrate type [29, 30], with particular attention paid to the effects of interfacial scattering between graphene and its substrate [31], and other experimental parameters [32]. With minimal visible reflection, graphene transmission is remarkably high, making it an ideal candidate for transparent optoelectronic devices.

Considerable research efforts have demonstrated improved optical contrast between graphene and non-graphene areas for graphene detection. Gao et al reported better graphene detection when utilizing a range of light instead of one specific wavelength [33]. Various heat and chemical treatments can selectively oxidize copper beneath graphene through graphene grain boundaries [34, 35]. The optical difference between copper and copper oxide is then easily detectable. Hong et al considered graphene coverage using deposited masks and reactive ion etching to remove non-monolayer graphene areas on CVD samples [36]. Elementally sensitive techniques then revealed graphene coverage. While effective, these methods can degrade and/or destroy graphene. Contrast can also be improved by manipulating the final substrate. Capping Si with SiO₂ of a specific thickness improves optical contrast [37, 38]. Altering the final thickness of poly(methyl methacrylate) substrates can also increase contrast [39]. Placing graphene on specifically engineered substrates [40], including photonic crystals [41, 42], improves detection as well.

Optical contrast improvement is not limited to substrate choice. Lewis *et al* and Kong *et al* reported graphene detection using dark field microscopy, which is highly sensitive to small changes in surface topology [43, 44]. Graphene retains the roughness of the initial copper foil during CVD growth while uncovered copper regions are smoothed, meaning graphene detection is possible. Differential

interference contrast microscopy has also been employed to observe differences in surface features, which are then attributed to graphene [45]. However, much like atomic force microscopy, these techniques cannot easily distinguish between graphene vs other surface topological features, and so risk misattributing non-graphene-related surface roughness to the presence of graphene.

Chemically sensitive experimental techniques can provide more thorough graphene characterization but may require sampling from the assembly line when integrated into commercial manufacturing processes. Raman spectroscopy is well-documented and detects vibrational features within the graphene crystal lattice [46] although it is largely limited by its point-resolution [9]. Interference reflection spectroscopy shows impressive graphene detection in realtime on substrates with appropriate reflection contrast [47]. Huang *et al* reported fast graphene grain boundary detection using transient absorption spectroscopy, as graphene grain boundaries have different densities of states compared to pristine areas when using a complex setup [48].

In this article, we report a simple, spatially resolved transmission technique for graphene detection with automated data analysis. We tightly focus a 633 nm laser beam to $1/e^2$ beam width of $\sim 10 \ \mu m$ and power of \sim 3 mW. Using an automatic micrometer stage, we measure the optical transmission at rasterized locations across the sample. When combined with knowledge of the statistical distribution of transmission values typical of the substrate, this data can be used to assess graphene coverage and quality on different transparent substrates. This method can characterize large samples, >1 cm², and is not limited by the thickness or type of substrate, assuming the substrate is transparent. The experimental data are corroborated with simulated data, in which we probe the effects of the beam radius and optical step length on final image clarity. Using these collected transmission data, we create optical transmission and layer number maps that explicitly quantify graphene coverage over the substrate with spatial resolution theoretically down to the diffraction limit of the laser wavelength. This methodology provides information comparable to two-dimensional Raman spectroscopy mapping in a fraction of the data collection time. Our statistical analysis can be automated and allows graphene coverage fraction determination without user-input threshold values, a marked improvement over traditional image analysis methods. We also consider the relationship between the calculated probability density functions (PDFs) and the graphene feature length scales. These results and our model can be used to assess graphene coverage, layer number, and uniformity for commercial graphene manufacturing processes.

2. Methods

2.1. Graphene transfer to glass

CVD graphene samples of different layer numbers (ACS Graphene) were transferred to glass. CVD graphene samples were carefully flattened in between two clean glass slides. Twenty microliters of 20 wt% poly(methyl methacrylate) (PMMA) (Sigma-Aldrich, 200336) in N-methyl-2-pyrrolidone were spin coated onto the graphene side of each sample to act as a support layer during transfer. Samples were annealed at 120 °C for 60 min. The copper substrates were removed via chemical etching in 0.4 M ammonium persulfate (Sigma-Aldrich, 215589) for 2 h. Remaining graphene/PMMA stacks were carefully transferred to fresh DI water to remove all ammonium persulfate. Samples were scooped on to glass slides. Slides were cleaned by oxygen plasma etching for 3 min using 450 W, soaking in basic hydrogen peroxide (pH 12) for 5 min, soaking in acidic hydrogen peroxide (pH 4) for 5 min, soaking in DI water for 10 min, and lastly patting dry. The PMMA support substrate was lastly removed by soaking the PMMA/graphene/glass stack in hot acetone.

Raman data to confirm the presence of graphene were collected on a WiTec confocal Raman spectroscopy instrument using a 532 nm laser source with a diameter of a few microns.

2.2. Spatially resolved optical transmission set up and analysis

The full beam path is shown in figure 1. A HeNe laser at 632.8 nm (ThorLabs, HNL150L) is spatially cleaned using a 75 μ m pinhole and two lenses with focal lengths of 50 and 75 mm before and after the pinhole, respectively, to remove unwanted higher order modes and expand the beam to a 1/e2 width of \sim 550 μ m. The beam of power P_0 is split using a 0.5 inch non-polarized beam splitter (ThorLabs, BS040) and the incident beam power $P_{\rm I}$, which is equivalent to ηP_0 where η accounts for the beam splitter fraction, is measured by focusing on a largearea Si detector (ThorLabs, PDA100A2). The remaining beam, $(1 - \eta)P_0$, is focused to a $1/e^2$ width of 10 μ m using a 36× infinity background corrected reflective objective lens (Newport, 50102-02) with a power efficiency of γ . The focused beam of power $\gamma(1-\eta)P_0$ passes through a specific location on a sample mounted on an automatic micrometer stage (Newport, ESP301) 10.4 mm away from the lens. Samples were mounted on glass or quartz slides to prevent sliding during data collection. Some polymer samples were sandwiched between glass or quartz slides to ensure surface planarity. The transmitted beam power, P_D , is measured by focusing on another large-area Si detector (ThorLabs, PDA100A2). The stage then moves an inputted optical step length and transmission at a different location on the sample is considered. The beam path, objective lens, and

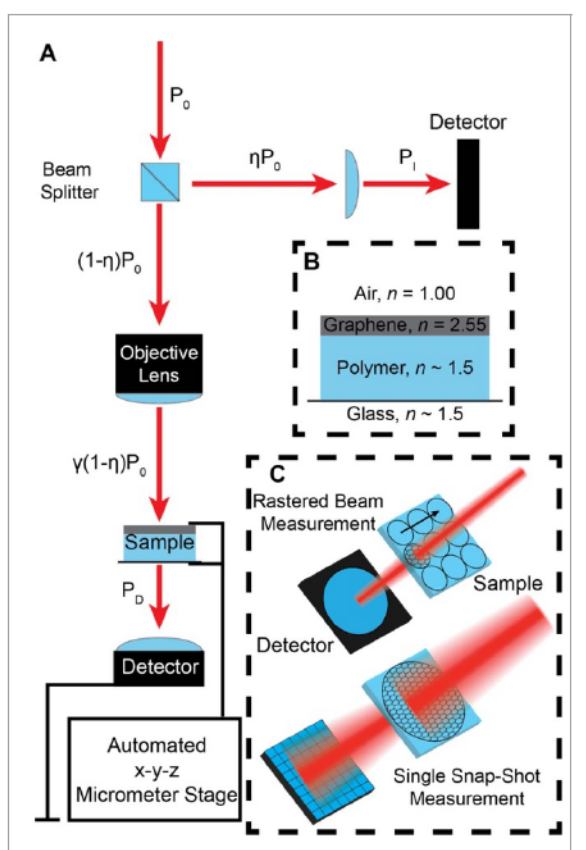


Figure 1. Schematic (a) of spatially resolved optical transmission set up where an incident beam of power Po passes through a beam splitter. A portion of the beam, ηP_0 , is measured as the incident power, PI. The remainder of the beam, $(1 \quad \eta)P_0$, is focused to a $1/e^2$ beam radius of 10 μ m using an objective lens. The tightly focused beam of power $\eta)P_0$ passes through a specific location on the mounted sample and the transmitted power, PD, is detected on a stationary detector. The sample then moves and another location is considered. Cross section of typical sample (b). Methodology difference between rastered measurement technique (used to measure all data in this paper) and the proposed snapshot variation of this technique, which uses a pixelated detector and may be more amenable to in-line measurements of a commercial process (c).

final detector remain stationary. Transmission data are calculated using the transmitted beam powers and the incident beam powers. For this wavelength and beam waist, the Rayleigh range is $z_0=243~\mu\mathrm{m}$ and the beam depth of focus is thus 486 $\mu\mathrm{m}$. Beam expansion through the graphene thickness is minimal. The slight expansion through the substrate can be accounted for by measuring a substrate background although we focus primarily on transmission through the graphene itself.

Data were collected in LabView using a program developed in-house. Detector voltage values were converted to power via P = V - (c/GR), where V is the measured voltage, c is an offset to account for the background voltage, G is the transimpedance gain of the detector, and R is the detector responsivity. Detectors were set to gain = 0, meaning $G = 1.53 \times 10^3 \text{ V A}^{-1}$. The detector responsivity at 633 nm is 0.425 A W⁻¹.

Power values were collected for 100 counts using a frequency of 500 Hz. These values balance accurate power collection and overall experiment time (supporting information (is available online at https://stacks.iop.org/2DM/8/025001/mmedia)). The objective lens efficiency, γ , was determined before each measurement using the incident beam power and transmitted beam power through a nonsample (NS) area, i.e. through the glass support, such that

$$\gamma = \frac{\eta}{(1-\eta)} \frac{P_{D,NS}}{P_{I,NS}}.$$
 (1)

Correction values hover near 0.538 \pm 0.0006 (supporting information). The final experimental transmissions through a sample sitting on top of a NS substrate (S + NS) was then calculated using

$$T = \frac{\eta}{\gamma (1 - \eta)} \frac{P_{D,S+NS}}{P_{I,S+NS}} = \frac{\eta}{\frac{\eta}{(1 - \eta)} \frac{P_{D,NS}}{P_{I,NS}} (1 - \eta)} \frac{P_{D,S+NS}}{P_{I,S+NS}}$$
$$= \frac{P_{I,NS}}{P_{D,NS}} \frac{P_{D,S+NS}}{P_{I,S+NS}}.$$
 (2)

Data analyses were completed in Python using a program developed in-house. Substrate sample edges were determined by examining a loss in transmitted power consistent with diffuse scattering off of the sample edge. These edges were used isolate sample transmission values. The PDF of each data set was calculated using the statsmodels package [49], which uses a kernel density estimation based on a Gaussian kernel and a rule of thumb bandwidth estimation based on default parameters. Resulting PDFs were fit to Gaussians using a minimization of the sum of squares. From these fitted peak centers, which correspond to transmission values, the probability of graphene's presence was determined. For monolayer graphene samples, the graphene coverage fraction was calculated by dividing the probability density values for graphene-assigned peaks by the sum of all of the probability density values. The uncertainty in the coverage was calculated using bootstrap methodology [50].

The difference in transmission between sample areas containing one layer of graphene and areas containing no graphene changes depending on the substrate used, as graphene absorbance varies. Specific absorbance values were calculated using

$$A = \frac{4adnn_0}{(n_0 + n_2 + adn)^2}$$
 (3)

where $adn = e^2/4\epsilon_0\hbar c = 0.0229253$, n = refractive index of graphene, d = thickness of the multilayer graphene, a = the absorption coefficient of graphene, $n_0 = \text{refractive index material above graphene}$, and $n_2 = \text{refractive index material below graphene}$, as derived by Holovsky *et al* [30]. Differences in

transmission due to multiple layers of graphene were calculated directly via

$$T = \left(1 + \frac{1.13}{2}\pi\alpha N\right)^{-2} \tag{4}$$

where α is the fine structure constant and N is the number of layers [28].

2.3. Simulation set up and analysis

A vectorized code written in Python was used to model the previously described spatially resolved optical transmission experiment. A laser beam of an inputted $1/e^2$ beam radius, r, was rasterized across a sample of specified dimensions using a chosen optical step length. For each beam position, as determined by the optical step length and sample dimensions, the incident beam power, P, was calculated [51] as a function of the distance between the location coordinate, d, and the beam center, μ , using the beam σ defined as $\sigma = 2r$ [51], via

$$P(x) = \frac{1}{\sqrt{2\pi\sigma^2}} e^{-(x-\mu)^2/2\sigma^2}.$$
 (5)

Locations within 3σ of each beam center were considered. The transmitted power was calculated using both the calculated incident power and an inputted transmission pattern. The PDFs of these simulated data were determined and fitted using the methodology previously described.

3. Results and discussion

Experimentally, we first assess uniform graphene coverage. The optical transmission of nominally ten layers of graphene on poly(ethylene terephthalate) (PET) was measured using a 1/e² beam radius of 7 μ m and an optical step length of 50 μ m (figure 2(a)). The uncertainty of these measured data are limited by the fractional volt uncertainty of the detectors used, which is \pm 0.018% for our setup, and the fractional position uncertainty of the micrometer stage, which is $\pm 1\%$. Such detection limits are similar to other graphene characterization methods, such as Raman spectroscopy and optical microscopy. Data are normalized such that transmission through the NS substrate is 1. Transmission through the sample substrate may be lower than 1 if other contaminates are present. We observe two primary transmission values (figure 2(b)) at 0.778 and 0.992. Assuming the higher transmission peak describes transmission through non-graphene polymer areas, the lower peak corresponds to transmission through graphene sections. Using equation (4), the predicted transmission for ten layers of graphene is 0.783, which is in excellent agreement with the experimentally determined transmission. Using the transmission values and rearranging equation (4), we calculate the number of layers of graphene present at each measured pixel (figure 2(c)). The layer number is largely consistent

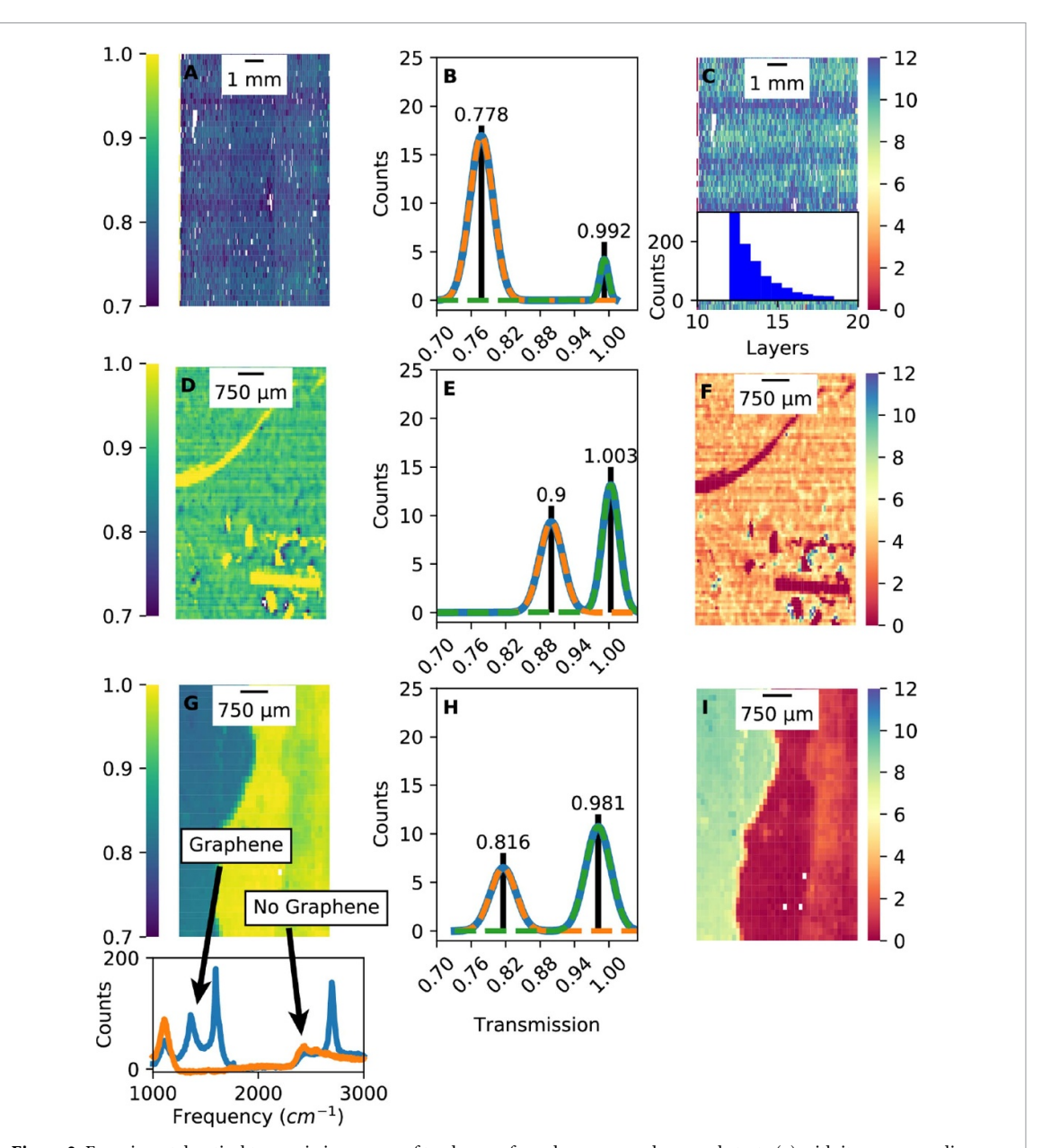


Figure 2. Experimental optical transmission maps: of ten layers of graphene on a polymer substrate (a) with its corresponding probability density function (b), and graphene layer number map (c) including histogram inset of layer values greater than 12; four layers of graphene on glass (d) with its probability density function (e) and layer number map (f); and eight layers of graphene on glass (g) as confirmed with Raman spectroscopy (inset) with its probability density function (h) and layer number map (i). Calculated probability density functions fitted with normal Gaussians provide prominent transmission values, which are useful for quality assessment. Transmission data less than 40% are likely non-sample contaminates, such as dust, and were removed.

across the sample area as well and hovers around ten layers. A few locations across the sample show more than 12 layers of graphene present (figure 2(c), inset). These values occur at locations of low transmission and are likely not graphene. Instead, they are probably NS contaminates, such as dust. Slight fluctuations appear in the measured transmissions and are from minor sample movement during the measurement. Using one set of measured data, we can definitively characterize the number of graphene layers present, the coverage fraction, and the coverage area.

Next we experimentally consider a sample with inconsistent graphene coverage. Using a beam radius

of 7 μ m and an optical step length of 55 μ m, we measured the optical transmission of four layers of graphene on glass (figure 2(d)). The PDF (figure 2(e)) shows two primary transmission values at 0.900 and 1.003, which correspond to graphene sitting on top of glass and the plain glass substrate respectively, as equation (4) predicts transmission through four layers of graphene to be 0.904 and non-graphene substrate areas were normalized to transmission = 1. By again rearranging equation (4), we directly calculate the number of layers of graphene at each measured pixel and present a layer coverage map (figure 2(f)). Usefully, our spatially resolved optical transmission

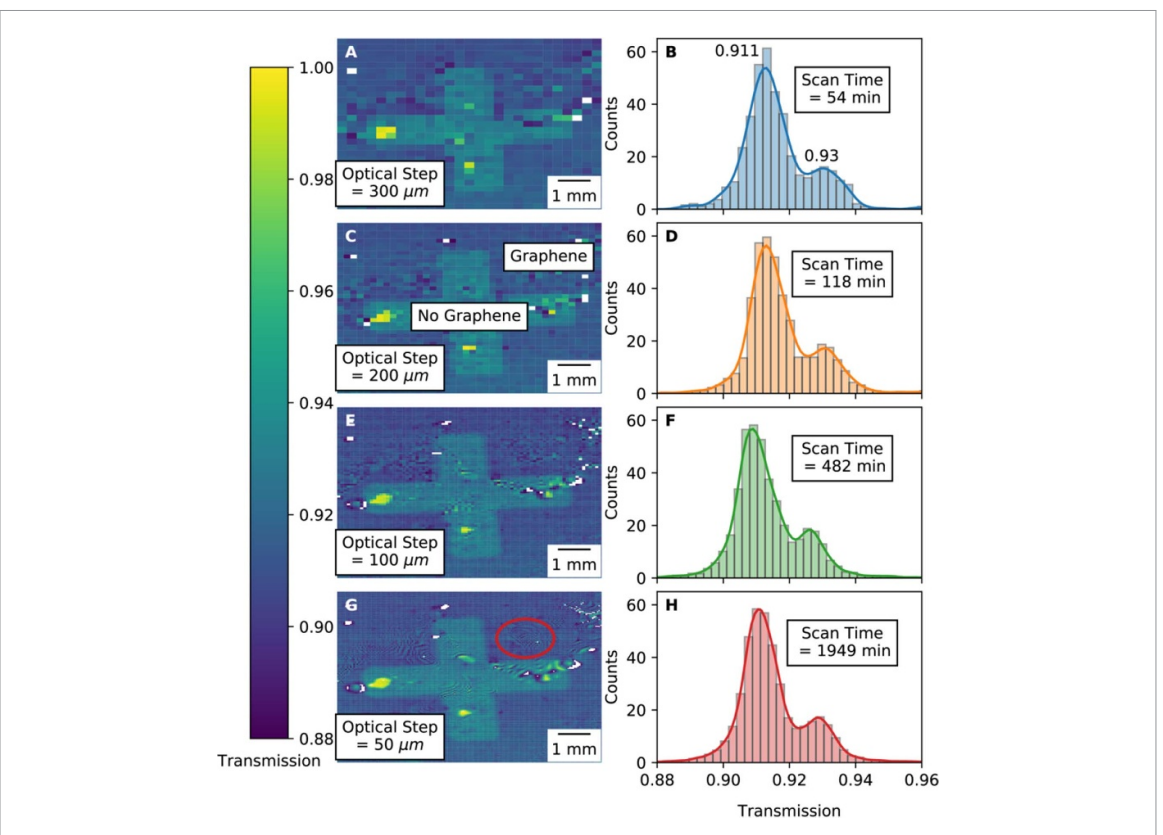


Figure 3. Optical transmission of macro-patterned graphene on poly(vinyl butyral) measured with a $1/e^2$ beam radius of 8 μ m and an optical step length of: 300 μ m (a) with its corresponding probability density function (PDF) (b); 200 μ m (c) with its corresponding PDF (d); 100 μ m (e) with its corresponding PDF (f); and 50 μ m (g) with its corresponding PDF (h).

method can quantify the success of the transfer process. Most areas in figure 2(f) show four layers of graphene are present. Barren areas where graphene transfer was unsuccessful are easily identifiable in both the transmission data and final layer map. In a previous work [11], we compared this coverage analysis to Raman measurements and found exceptional agreement, implying that our optical transmission method can reliably detect the graphene coverage fraction. Thus, transfer success can be considered by measuring both graphene coverage and layer consistency in a non-destructive manner. We also compare our optical transmission map to two-dimension Raman mapping over three notable graphene peaks, D, G, and 2D in the supporting information and demonstrate layer agreement.

We highlight the ability of our spatially resolved optical transmission method to determine graphene edges by experimentally measuring the optical transmission of eight layers of graphene on glass using a $1/e^2$ beam radius of 8 μ m and an optical step length of 100μ m (figure 2(g)). We see two very distinct regions with transmissions of 0.816 and 0.981 that are highlighted in the calculated PDF (figure 2(h)). We attribute the higher transmission peak to pixels describing plain glass and the lower transmission peak to pixels describing eight layers of graphene deposited on plain glass. These assumptions are confirmed with Raman spectroscopy (figure 2(g), inset), which shows the

characteristic D, G, and 2D graphene peaks at 1360, 1595, 2695 cm⁻¹, respectively [46]. Via equation (4), we expect the transmission of eight layers of graphene to be 0.821, which agrees well with our experimental data. The small deviation may be due to residual poly(methyl methacrylate) remaining after the transfer process. Additional studies can consider detecting sacrificial polymer residues on graphene samples post-transfer. We map the layer number across the entire measured sample in figure 2(i). As expected, we see a clear region where eight layers of graphene are present. There is a well-defined edge between the graphene and glass background substrate where the number of layers transitions from 8 to 0. The slight change in transmission across the plain substrate is attributed to residue on the glass itself introduced after transfer and is considered within the widths of the PDF peaks, a feature of this analysis method. These data in particular highlight the ability of our spatially resolved optical transmission method to determine graphene area edges, an important consideration in large-scale transfer where edge effects can impact the graphene performance.

Our optical transmission analysis considers the PDF of each measured data set to obtain prominent transmission values. For graphene samples on consistent substrates, two major transmissions are determined and correspond to transmission through the substrate and transmission through

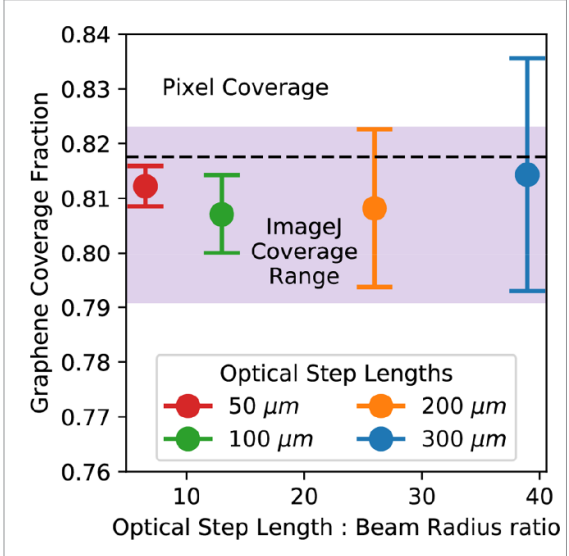
graphene sitting on top of the substrate. We verify this by calculating the absorbance of graphene, which depends on the number of layers present, via equation (3). We also consider samples where the transmission through the plain substrate varies. A macro-patterned monolayer graphene sample was transferred to poly(vinyl butyral) and the optical transmission was measured using a 1/e² beam radius of 8 μ m and different optical step lengths (figure 3). The largest optical step length of 300 μ m yields a low-resolution transmission map where the pattern is difficult to distinguish (figure 3(a)). The high transmission spots of ~ 1 are artifacts from the macropattern process where a pocket of air remains trapped between the glass slides. We calculate the PDF of the optical transmission data (figure 3(b)) and determine two major transmission peaks at 0.911 and 0.930. Using equation (3) and assuming the index of refraction of poly(vinyl butyral) [52] is 1.48 and the index of refraction of plain glass [53] is 1.54, monolayer graphene absorbs 1.52% of incoming light when placed on poly(vinyl butyral). The higher transmission value of 0.93 describes sample areas where only the polymer background is present. We expect areas containing graphene and the polymer to have transmission values of 0.930 - 0.0146 = 0.915, which agrees well with the measured transmission of 0.911.

Decreasing the optical step length to 200 μ m, 100 μ m, and lastly 50 μ m (figures 3(c), (e) and (g)) increases the resolution of the final image by increasing the number of descriptive pixels. Consequently, smaller step lengths show better image clarity and can even distinguish thin-film diffraction rings present from the interaction of the sample with its support glass slides (figure 3(g)). Despite this improvement, the optical step length has minimal impact on the calculated PDFs with regards to PDF shape and prominent features (figures 3(d), (f) and (h)). Decreasing the optical step length increases sample measurement time, as each individual pixel takes about 4 s to measure. The lowest resolution sample, completed with an optical step length of 300 μ m, took around 54 min to obtain. Using a much smaller optical step length of 50 μ m greatly increased data collection time to 1949 min. Comparatively, we see a 6× improvement in image clarity at the expense of a 36× increase in data collection time. The snapshot variation of the technique suggested in figure 1(c) would overcome these measurement time challenges.

From each PDF, we calculate the graphene coverage fraction by dividing the probability density values for the graphene peaks by all of the probability density values. This metric describes the sample area covered by graphene and is determined from the PDF. Typical image analysis methods to assess coverage fractions cannot automatically distinguish between graphene and non-graphene areas without specific user input, usually in the form

of threshold cutoffs. Image-based coverage calculations can also become more complicated when considering samples with non-uniform backgrounds, as the threshold limits vary across the sample area. Our coverage calculation eliminates user-specified thresholds. Background variation is captured within the width of each peak in the calculated PDF. We reasonably assign the highest transmission peak to sample areas of the pure background, meaning the remaining lower transmission peak must describe areas with graphene and the background. Graphene layer number variation is captured in this analysis by additional lower transmission peaks.

To verify our coverage calculation, we process the highest resolution optical transmission image, collected using an optical step length of 50 μ m (figure 3(g)), with ImageJ [54] to determine the graphene coverage fraction. Visually, two brightness cutoff values, after converting the image to grayscale, appeared reasonable, 97 and 98. From these, we determine a coverage fraction range between 0.791 and 0.823, respectively (figure 4). We also calculate the graphene coverage fraction by counting the number of image pixels above a set threshold, which we determine as the intersection between the two peaks of calculated PDF. At this point, the likelihood the pixel contains graphene and the polymer and the likelihood the pixel contains only polymer are equal. The graphene coverage fraction via pixel counting is 0.818. We present the coverage fractions calculated using our PDF analysis plotted over the optical step length to 1/e² beam radius (figure 4). Specifically, we find the graphene coverages are 0.814 ± 0.022 , 0.813 ± 0.022 , 0.807 ± 0.0071 , and 0.812 ± 0.0036 , for optical step lengths of 300 μ m, 200 μ m, 100 μ m, and 50 μ m, respectively. Our PDF calculated coverage fractions all fall within the coverage range determined via ImageJ. Most values also show excellent agreement with the coverage determined via pixel counting. As expected, increasing the resolution of the image by using a smaller optical step length significantly decreases the uncertainty in calculated coverage values by improving the image clarity. Notably, even the larger optical step lengths provide reliable coverage values with very low uncertainties. Our coverage determination provides useful graphene coverage information from collected transmission images without relying on user-inputted thresholds. As shown, ImageJ analysis can generate a range of acceptable coverages because the thresholds are static and determined by the user. Pixel counting methodology also requires a user threshold and fails to differentiate between different layers of graphene coverage. Our PDF coverage analysis can be automated based on peak assignments and can calculate coverage for regions with different layers of graphene, in contrast to the pixel-counting and threshold approaches used in ImageJ.



IOP Publishing

Figure 4. Graphene coverage fractions calculated using probability density functions for macro-patterned graphene on poly(vinyl butyral) as plotted over the optical step length to $1/e^2$ beam radius ratio. Data were collected using a $1/e^2$ beam radius of 8 μ m. Error bars are calculated via the bootstrap method. The coverage fraction range determined via ImageJ (purple region) and coverage fraction calculated via pixel counting above a set threshold (black dashed line) are shown.

Our analysis method depends on considerable distinction between graphene and non-graphene pixels. While some PDF peak overlap is acceptable, generally the background must be consistent enough to distinguish between sample and NS areas. To highlight this, we present experimental data collected on a very inhomogeneous poly(methyl methacrylate) substrate, measured using an optical step length of 75 μ m and a 1/e² beam radius of 7 μ m (figure 5). The image obtained with our spatially resolved optical transmission technique reveals sample areas ranging in transmission from 1 to 0.8 (figure 5(a)). Some pixels show lower transmissions around 0.6. Correspondingly, the calculated PDF covers a range of transmission values (figure 5(b)). Because the spread in transmission values approaches 20% and graphene absorbance is nearly 1%-2%, graphene detection on this particular substrate is not possible. We posit our optical transmission data could be used to calculate surface roughness although this method requires additional modeling and analysis.

In addition to these experimental measurements, we also simulate our spatially resolved optical transmission process to understand the effects of the 1/e² beam radius and the optical step length on the final clarity and on the calculated PDF of the data. We rasterized beam radii of different sizes across a simulated macro-patterned graphene sample using different optical step lengths and calculated the optical transmission (figure 6). The background transmission does not vary and is conveniently set to 1. Using equation (3) and assuming the refractive index of

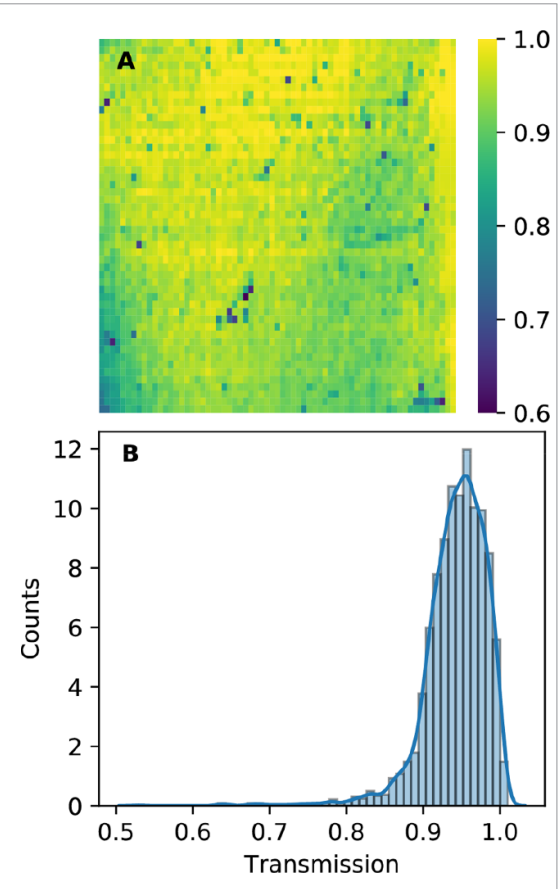


Figure 5. Experimentally collected optical transmission data of a plain poly(methyl methacrylate) substrate measure using a $1/e^2$ beam radius of 7 μ m and an optical step length of 75 μ m (a) and corresponding probability density function and histogram (b).

the background is 1.458, i.e. quartz glass [55], the absorbance of monolayer graphene is 1.56%, meaning transmission through graphene areas becomes 1 - 0.0156 = 0.984. The largest beam radius of 100 μ m and optical step length of 100 μ m produced a low-resolution image (figure 6(a)) with poor clarity. Decreasing the step length to 50 μm (figure 6(b)) and 25 μ m (figure 6(c)) only marginally improves the overall image resolution and quality. For these data, the large beam radius cannot distinguish clearly between graphene and non-graphene areas. The edges between these areas show intermediate transmission values, as part of the laser beam passes through graphene/polymer portions while part of the beam passes through pure polymer portion. These values are highlighted in the calculated PDF and histogram (figure 6(a), inset). Consequently, decreasing the optical step length does not improve the final image quality despite increasing the number of pixels in the image.

Decreasing the beam radius to 50 μ m and considering a larger optical step length of 100 μ m (figure 6(d)) improves image quality even though the beam itself extends beyond the measurement area of each pixel. We observe a reduction in intermittent transmissions compared to the previous larger beam

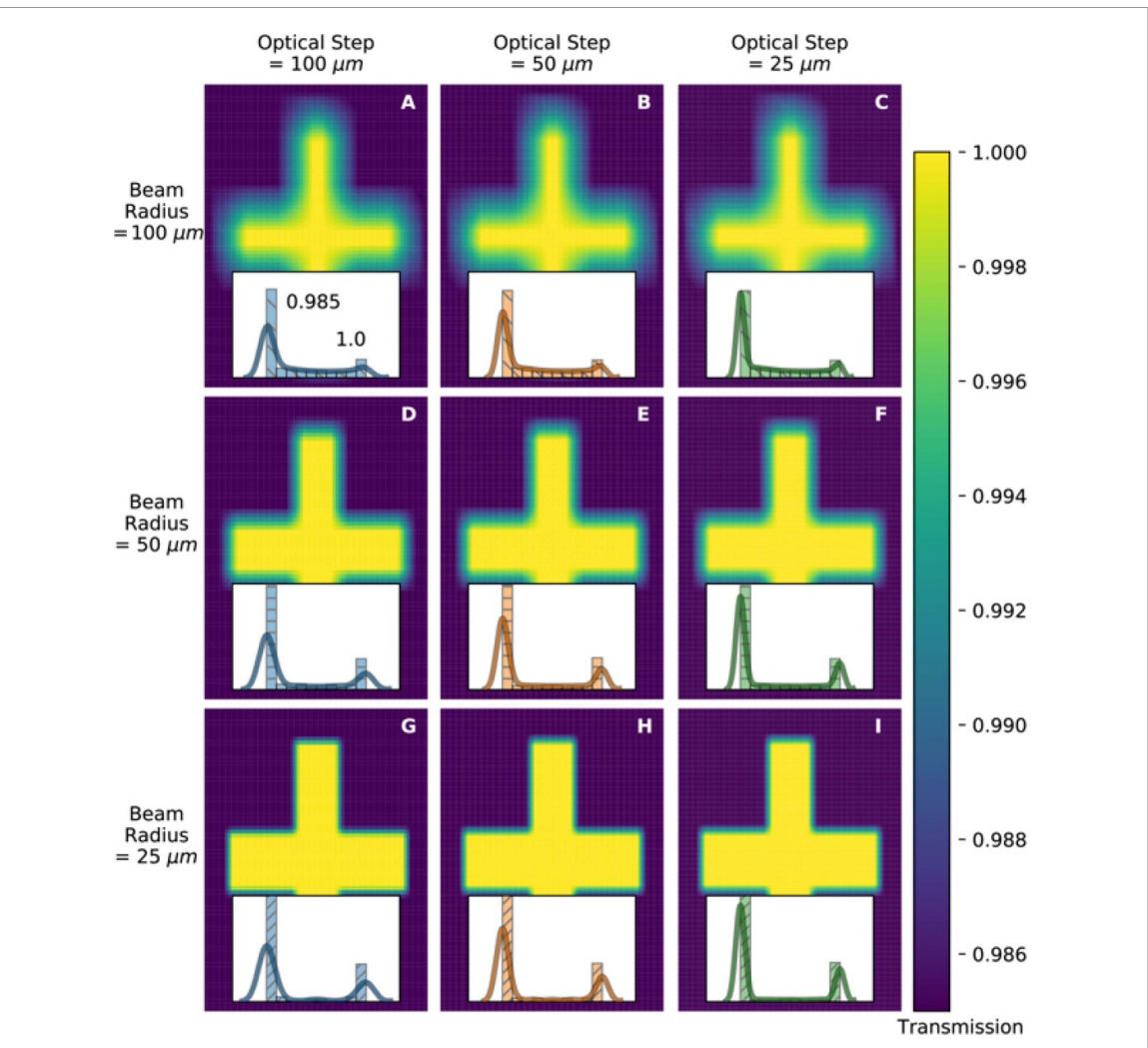


Figure 6. Simulated optical transmission data of macro-patterned graphene on plain substrate with no background variation using: $1/e^2$ beam radius = $100~\mu$ m, optical step length = $100~\mu$ m (A); $1/e^2$ beam radius = $100~\mu$ m, optical step length = $50~\mu$ m (b); $1/e^2$ beam radius = $100~\mu$ m, optical step length = $50~\mu$ m (c); $1/e^2$ beam radius = $50~\mu$ m, optical step length = $100~\mu$ m (d); $1/e^2$ beam radius = $50~\mu$ m, optical step length = $50~\mu$ m (e); $1/e^2$ beam radius = $50~\mu$ m, optical step length = $25~\mu$ m (f); $1/e^2$ beam radius = $25~\mu$ m, optical step length = $100~\mu$ m (g); $1/e^2$ beam radius = $25~\mu$ m, optical step length = $50~\mu$ m (h); and $1/e^2$ beam radius = $25~\mu$ m, optical step length = $25~\mu$ m (i). Calculated probability density functions and histograms are included in each inset.

radius although decreasing the optical step length to $50 \mu m$ (figure 6(e)) and 25 μm (figure 6(f)) does not significantly affect overall image clarity. We obtain the best image quality for our highest resolution samples calculated with a beam radius of 25 μ m and optical step lengths of 100 μ m (figure 6(g)), 50 μ m (figure 6(h)), and 25 μ m (figure 6(i)). The number of intermediate transmission values that lie between 1 and 0.984 is significantly reduced and the edges of the pattern are obvious. We posit that oversampling using a large beam radius and a smaller optical step length is not necessary to improve overall image clarity and quality. A beam radius equivalent to the optical step length yields the most descriptive data in that the pixel area is fully considered by the beam. Larger optical step lengths can also be used with a small beam if the sample is relatively uniform, meaning the small area directly measured by the beam can describe the larger pixel accurately.

Lastly, we consider the effect of the graphene feature length on the shape of the obtained PDF using our optical transmission model. We simulate patches of different length scales of monolayer graphene on an arbitrary substrate using an optical step length of 15 $\mu\mathrm{m}$ and a 1/e² beam radius of 10 μ m and a constant graphene area coverage fraction of 20% (figure 7). We assume the absorbance of graphene in this case is 2.5%. For the smallest feature case of 100 μ m (figure 7(a)), a range of transmission values between the expected transmission through monolayer graphene on a substrate, 0.975, and the expected transmission through the plain substrate, 1.000, are observed. This is highlighted in the calculated PDF (figure 7(b)). Likely, the small beam radius and optical step length are unable to exactly locate pure graphene areas and instead hit graphene patch edges. The observed transmission then changes depending on the portion of graphene

IOP Publishing 2D Mater. **8** (2021) 025001 A J Carr *et al*

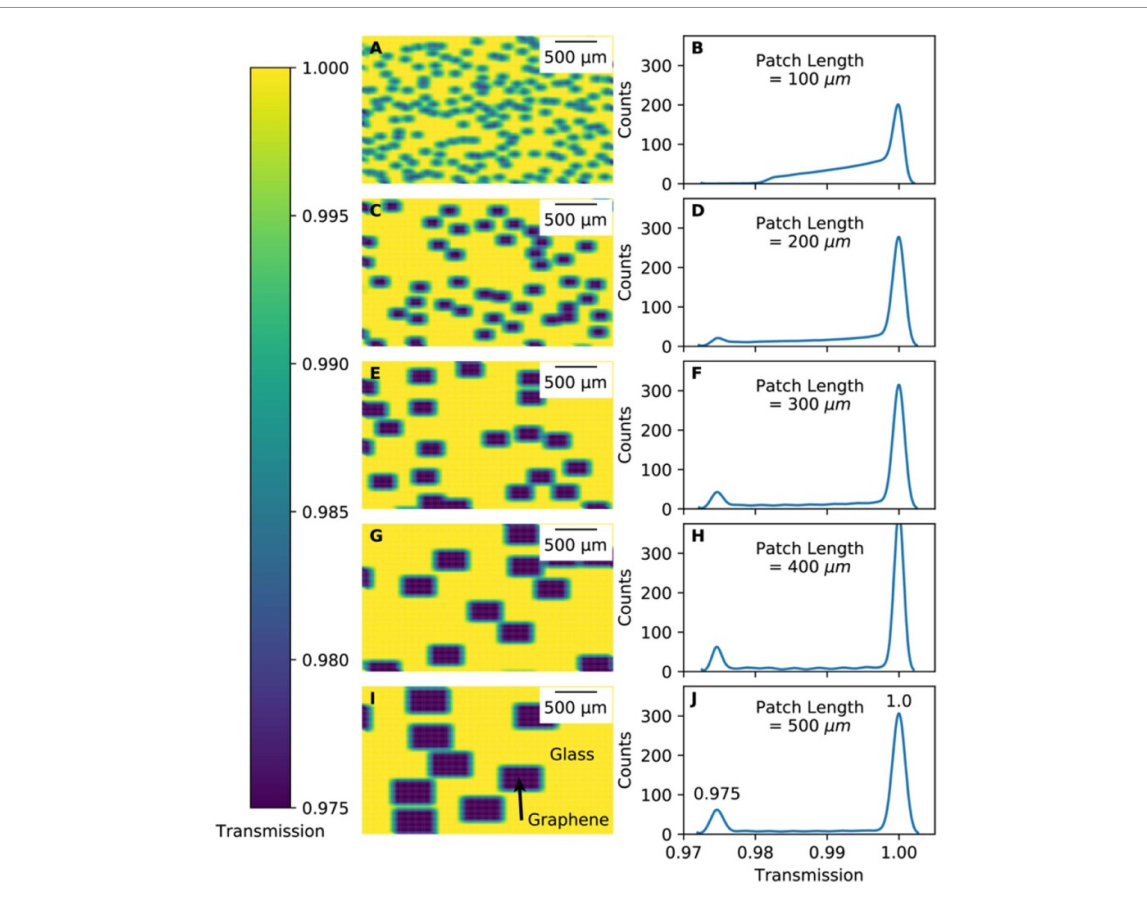


Figure 7. Simulated optical transmission data of monolayer graphene on an arbitrary substrate for graphene patch lengths of: $100~\mu\text{m}$ (a) with corresponding calculated probability density function (PDF) (b); $200~\mu\text{m}$ (c) with corresponding PDF (d); $300~\mu\text{m}$ (e) with corresponding PDF (f); $400~\mu\text{m}$ (g) with corresponding PDF (h); and $500~\mu\text{m}$ (i) with corresponding PDF (J). Data were simulated using an optical step length of $15~\mu\text{m}$ and a $1/e^2$ beam radius of $10~\mu\text{m}$. The graphene coverage area was held constant at 20% for all cases. The absorbance of graphene was assumed to be 2.5.

vs non-graphene area occupied by the beam during the measurement. Nearly zero areas are observed that are entirely covered by graphene, as noted by the lack of dark purple regions in figure 7(a), although most graphene areas show intermediate edge transmissions. This effect is lessened when we increase the graphene feature size to 200 μ m (figures 7(c) and (d)). The PDF shows two distinct peaks at 0.975 and 1.000, as expected for monolayer graphene on our substrate, and the plain substrate, respectively. We also observe additional intermediate transmissions in between these expected values though, as the beam samples some graphene patch edges. Increasing the feature size length to 300 µm mitigates intermediate transmission value measurements (figures 7(e) and (f)) and by 400 μ m almost all measured data occur at either 0.975 or 1.000 (figures 7(g) and (h)). The largest measured patch length, 500 μ m, also shows nearly no edge transmission data (figures 7(i) and (j)). Instead, the beam can readily distinguish between graphene and non-graphene areas. This is probably because there are fewer edges present over the sample surface area for these larger feature samples, meaning the likelihood the beam happens to fall on a transition from graphene to the

glass substrate is lower. With a greater number of data registering as either exactly 0.975 or 1.000, the PDF will show fewer intermediate transmission values. This analysis is particularly useful when characterizing samples with unknown feature size lengths, as one could model the inputted experimental parameters and then vary the input patch length to obtain the likely feature size.

4. Conclusions

Large-scale in-line detection of graphene on transparent substrates is critical to future commercial graphene application development. Many existing techniques rely on optical contrast manipulation and require user-inputted thresholds to locate graphene on measured samples, or are inherently destructive. In this paper, we present a simple, spatially resolved optical transmission method to determine graphene coverage and layer number over different transparent substrates, including polymer films and glass. Our automated analysis uses PDFs to map graphene layer values over entire sample areas and to calculate total graphene area coverage. This technique is not limited to specific substrate types or

thicknesses but requires substrates to be reasonably uniform. Excessively rough substrates may diffusely scatter light thus impeding the transmission measurement process. Future research will model diffuse scattering off of sample surfaces to assess surface roughness. This approach of accounting for diffuse scattering may enable novel application of the technique we have presented, such as the characterization of graphene doped with heteroatoms. Because this method relies on optical transmission, graphene layer numbers up to the asymptotic limit of transmission through graphene, stated in equation (4), can be considered. We demonstrate excellent graphene coverage agreement with traditional image-based analyses and have previously shown agreement with Raman-based analysis [11]. In this work, we utilize a rastered laser beam across sample area to provide high-precision data. Our analysis and methodology could easily be applied to pixelated image sensors to provide the same information in a shorter time.

Additionally, we corroborate our experimental results with simulated data to consider the effects of different experimental parameters on measurement quality. Our model provides reasonable guidelines to assess graphene coverage, layer number, and typical feature size, a useful tool when characterizing transferred samples. Future research will develop a maximum likelihood analysis to determine graphene feature sizes using one set of measured data with specific inputted experimental parameters.

Acknowledgments

This research used resources of the Center for Functional Nanomaterials, which is a U.S. DOE Office of Science Facility, at Brookhaven National Laboratory under Contract No. DE-SC0012704. Partial support for A J C was provided by the National Science Foundation through awards CBET-1335787 and CBET-1903189 and the Petroleum Research Fund award 55729-ND9. This research used resources of the Center for Functional Nanomaterials, which is a U.S. DOE Office of Science Facility, at Brookhaven National Laboratory under Contract No. DE-SC0012704. Partial support for AJC was provided by the National Science Foundation through awards CBET-1335787 and CBET-1903189 and the Petroleum Research Fund award 55729-ND9. We thank Dr Mira Baraket and Greg Erickson of General Graphene Corp. for custom sample preparation.

ORCID iDs

Amanda J Carr https://orcid.org/0000-0002-8224-7677

Matthew D Eisaman https://orcid.org/0000-0002-3814-6430

References

- [1] Wang X, Liu A, Xing Y, Duan H, Xu W, Zhou Q, Wu H, Chen C and Chen B 2018 Three-dimensional graphene biointerface with extremely high sensitivity to single cancer cell monitoring *Biosens. Bioelectron.* 105 22–28
- [2] Park J *et al* 2018 Soft, smart contact lenses with integrations of wireless circuits, glucose sensors, and displays *Sci. Adv.* 4 eaap9841
- [3] Kireev D and Offenhäusser A 2018 Graphene & two-dimensional devices for bioelectronics and neuroprosthetics 2D Mater. 5 042004
- [4] Peng P, Li L, He P, Zhu Y, Fu J, Huang Y and Guo W 2019 One-step selective laser patterning of copper/graphene flexible electrodes *Nanotechnology* 30 185301
- [5] Jo G, Choe M, Lee S, Park W, Kahng Y H and Lee T 2012 The application of graphene as electrodes in electrical and optical devices *Nanotechnology* 23 112001
- [6] Dissanayake D M N M and Eisaman M D 2016 Chemical-free n-type and p-type multilayer-graphene transistors Appl. Phys. Lett. 109 053110
- [7] Hecht D S, Hu L and Irvin G 2011 Emerging transparent electrodes based on thin films of carbon nanotubes, graphene, and metallic nanostructures Adv. Mater. 23 1482–513
- [8] Dissanayake D M, Ashraf A, Dwyer D, Kisslinger K, Zhang L, Pang Y, Efstathiadis H and Eisaman M D 2016 Spontaneous and strong multi-layer graphene n-doping on soda-lime glass and its application in graphene-semiconductor junctions Sci. Rep. 6 21070
- [9] Deng B, Liu Z and Peng H 2018 Toward mass production of CVD graphene films Adv. Mater. 31 1800996
- [10] Polsen E S, McNerny D Q, Viswanath B, Pattinson S W and John Hart A 2015 High-speed roll-to-roll manufacturing of graphene using a concentric tube CVD reactor Sci. Rep. 5 10257
- [11] Carr A J, Head A, Boscoboinik J A, Bhatia S R and Eisaman M D 2020 Direct evidence of graphene-induced molecular reorientation in polymer films Adv. Mater. Interfaces 7 2000113
- [12] Qi Z, Zhu X, Jin H, Zhang T, Kong X, Ruoff R S, Qiao Z and Ji H 2018 Rapid identification of the layer number of large-area graphene on copper Chem. Mater. 30 2067–73
- [13] Jia C, Jiang J, Gan L and Guo X 2012 Direct optical characterization of graphene growth and domains on growth substrates *Sci. Rep.* 2 707
- [14] Zhang G, Guell A G, Kirkman P M, Lazenby R A, Miller T S and Unwin P R 2016 Versatile polymer-free graphene transfer method and applications ACS Appl. Mater. Interfaces 8 8008–16
- [15] Leong W S et al 2019 Paraffin-enabled graphene transfer Nat. Commun. 10 867
- [16] Chandrashekar B N, Deng B, Smitha A S, Chen Y, Tan C, Zhang H, Peng H and Liu Z 2015 Roll-to-roll green transfer of CVD graphene onto plastic for a transparent and flexible triboelectric nanogenerator Adv. Mater. 27 5210–6
- [17] Cai C, Jia F, Li A, Huang F, Xu Z, Qiu L, Chen Y, Fei G and Wang M 2016 Crackless transfer of large-area graphene films for superior-performance transparent electrodes *Carbon* 98 457–62
- [18] Castro Neto A H, Guinea F, Peres N M R, Novoselov K S and Geim A K 2009 The electronic properties of graphene Rev. Mod. Phys. 81 109–62
- [19] Geim A K 2009 Graphene: status and prospects Science 324 1530–4
- [20] Novoselov K S, Fal'ko V I, Colombo L, Gellert P R, Schwab M G and Kim K 2012 A roadmap for graphene Nature 490 192–200
- [21] Dawlaty J M, Shivaraman S, Strait J, George P, Chandrashekhar M, Rana F, Spencer M G, Veksler D and Chen Y 2008 Measurement of the optical absorption spectra

- of epitaxial graphene from terahertz to visible *Appl. Phys. Lett.* **93** 131905
- [22] Mak K F, Sfeir M Y, Wu Y, Lui C H, Misewich J A and Heinz T F 2008 Measurement of the optical conductivity of graphene Phys. Rev. Lett. 101 196405
- [23] Lee C, Kim J Y, Bae S, Kim S K, Hong B H and Choi E J 2011 Optical response of large scale single layer graphene Appl. Phys. Lett 98 071905
- [24] Bruna M and Borini S 2009 Optical constants of graphene layers in the visible range *Appl. Phys. Lett.* **94** 031901
- [25] Nair R R, Blake P, Grigorenko A N, Novoselov K S, Booth T J, Stauber T, Peres N M and Geim A K 2008 Fine structure constant defines visual transparency of graphene Science 320 1308
- [26] Kravets V G, Grigorenko A N, Nair R R, Blake P, Anissimova S, Novoselov K S and Geim A K 2010 Spectroscopic ellipsometry of graphene and an exciton-shifted van Hove peak in absorption *Phys. Rev.* B 81 155413
- [27] Skulason H S, Gaskell P E and Szkopek T 2010 Optical reflection and transmission properties of exfoliated graphite from a graphene monolayer to several hundred graphene layers *Nanotechnology* 21 295709
- [28] Zhu S-E, Yuan S and Janssen G C A M 2014 Optical transmittance of multilayer graphene *Europhys. Lett.* 108 17007
- [29] Zhan T, Shi X, Dai Y, Liu X and Zi J 2013 Transfer matrix method for optics in graphene layers J. Phys. Condens. Matter 25 215301
- [30] Holovsky J, Nicolay S, De Wolf S and Ballif C 2015 Effect of the thin-film limit on the measurable optical properties of graphene Sci. Rep. 5 15684
- [31] Stauber T, Peres N M R and Geim A K 2008 Optical conductivity of graphene in the visible region of the spectrum Phys. Rev. B 78 085432
- [32] Abergel D S L, Russell A and Fal'ko V I 2007 Visibility of graphene flakes on a dielectric substrate Appl. Phys. Lett. 91 063125
- [33] Gao L, Ren W, Li F and Cheng H M 2008 Total color difference for rapid and accurate identification of graphene ACS Nano 2 1625–33
- [34] Cheng Y et al 2016 Direct identification of multilayer graphene stacks on copper by optical microscopy Chem. Mater. 28 2165–71
- [35] Duong D L *et al* 2012 Probing graphene grain boundaries with optical microscopy *Nature* 490 235–9
- [36] Hong K P et al 2019 Visualization of CVD-grown graphene on Cu film using area-selective ALD for quality management Appl. Surf. Sci. 496 143614
- [37] Ni Z H, Wang H M, Kasim J, Fan H M, Yu T, Wu Y H, Feng Y P and Shen Z X 2007 Graphene thickness determination using reflection and contrast spectroscopy *Nano Lett.* 7 2758–63
- [38] Blake P, Hill E W, Castro Neto A H, Novoselov K S, Jiang D, Yang R, Booth T J and Geim A K 2007 Making graphene visible Appl. Phys. Lett. 91 063124

- [39] Teo G, Wang H, Wu Y, Guo Z, Zhang J, Ni Z and Shen Z 2008 Visibility study of graphene multilayer structures J. Appl. Phys. 103 124302
- [40] Papasimakis N, Luo Z, Shen Z X, De Angelis F, Di Fabrizio E, Nikolaenko A E and Zheludev N I 2010 Graphene in a photonic metamaterial Opt. Express 18 8353–9
- [41] Chang K, Liu J T, Xia J B and Dai N 2007 Enhanced visibility of graphene: effect of one-dimensional photonic crystal Appl. Phys. Lett. 91 181906
- [42] Son J H, Baeck S J, Park M H, Lee J B, Yang C W, Song J K, Zin W C and Ahn J H 2014 Detection of graphene domains and defects using liquid crystals *Nat. Commun.* 5 3484
- [43] Lewis A M, Derby B and Kinloch I A 2013 Influence of gas phase equilibria on the chemical vapor deposition of graphene ACS Nano 7 3104–17
- [44] Kong X H, Ji H X, Piner R D, Li H F, Magnuson C W, Tan C, Ismach A, Chou H and Ruoff R S 2013 Non-destructive and rapid evaluation of chemical vapor deposition graphene by dark field optical microscopy *Appl. Phys. Lett.* 103 043119
- [45] Yang G and Kim J 2015 Probing patterned defects on graphene using differential interference contrast observation Appl. Phys. Lett. 106 081901
- [46] Malard L M, Pimenta M A, Dresselhaus G and Dresselhaus M S 2009 Raman spectroscopy in graphene *Phys. Rep.* 473 51–87
- [47] Li W, Moon S, Wojcik M and Xu K 2016 Direct optical visualization of graphene and its nanoscale defects on transparent substrates Nano Lett. 16 5027–31
- [48] Huang K C, McCall J, Wang P, Liao C S, Eakins G, Cheng J X and Yang C 2018 High-speed spectroscopic transient absorption imaging of defects in graphene *Nano Lett.* 18 1489–97
- [49] Seabold S and Perktold J 2010 Statsmodels: econometric and statistical modeling with python PROC. OF THE 9th PYTHON IN SCIENCE CONF. (SCIPY 2010) 9 92–96 http://conference.scipy.org/proceedings/scipy2010/pdfs/ seabold.pdf
- [50] Efron B and Tibshirani R J 1994 An Introduction to the Bootstrap (Boca Raton: Chapman & Hall/CRC)
- [51] Saleh B E A and Teich M C 1991 Fundamentals of Photonics (New York: Wiley)
- [52] El-Din N M S and Sabaa M W 1995 Thermal degradation of poly(vinyl butyral) laminated safety glass *Polym. Degrad.* Stab. 47 283–8
- [53] 2011 CRC Handbook of Chemistry and Physics (Boca Raton, FL: CRC Press) Havnes W M 978–1439855119
- [54] Schneider C A, Rasband W S and Eliceiri K W 2012 NIH Image to ImageJ: 25 years of image analysis *Nat. Methods* 9 671–5
- [55] Tan G L, Lemon M F, Jones D J and French R H 2005 Optical properties and London dispersion interaction of amorphous and crystalline SiO₂ determined by vacuum ultraviolet spectroscopy and spectroscopic ellipsometry *Phys. Rev.* B 72 205117